

RSC Advances



This is an *Accepted Manuscript*, which has been through the Royal Society of Chemistry peer review process and has been accepted for publication.

Accepted Manuscripts are published online shortly after acceptance, before technical editing, formatting and proof reading. Using this free service, authors can make their results available to the community, in citable form, before we publish the edited article. This *Accepted Manuscript* will be replaced by the edited, formatted and paginated article as soon as this is available.

You can find more information about *Accepted Manuscripts* in the [Information for Authors](#).

Please note that technical editing may introduce minor changes to the text and/or graphics, which may alter content. The journal's standard [Terms & Conditions](#) and the [Ethical guidelines](#) still apply. In no event shall the Royal Society of Chemistry be held responsible for any errors or omissions in this *Accepted Manuscript* or any consequences arising from the use of any information it contains.



Gold Microsheets Having Nano/Microporous Structures Fabricated by Ultrasonic-Assisted Cyclic Galvanic Replacement

P. Pienpinijtham,^{a,*} P. Sornprasit,^a K. Wongravee,^a C. Thammacharoen^a and S. Ekgasit^a

Received 00th January 20xx,
Accepted 00th January 20xx

DOI: 10.1039/x0xx00000x

www.rsc.org/

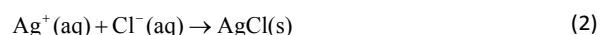
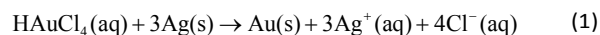
A novel technique for a fabrication of nano/microporous gold (Au) microsheets using ultrasonic-assisted cyclic Galvanic replacement reaction between sacrificed silver (Ag) plate and gold ion (AuCl₄⁻) is reported. At first, AuCl₄⁻ is reduced on the surface of sacrificed Ag *via* Galvanic replacement reaction. Then, the epitaxial growth of Au film on the Ag surface is disturbed by the precipitated AgCl byproduct of this Galvanic replacement reaction. The co-precipitated AgCl and Galvanic-generated Au nanostructures induce the formation of an interpenetrated Au/AgCl nanocomposite film on the surface of sacrificed Ag plate. Finally, the ultrasonic radiation enables an auto-detachment of the Galvanic-generated film along the AgCl/Ag interface. The Galvanic replacement and auto-detachment processes continuously occurs as a cycle until sacrificed Ag is totally consumed. The coral-like Au nanostructures with nano/microporous morphology are realized after removing AgCl by NH₃ treatment. The hierarchical nano/microporous structures have micropores and nanopores with the size of 0.15–0.30 μm and 30–60 nm, respectively, separated by chain-like Au structures. The complex porous structures with an easily flow-through of liquid provide potential applications as high-efficiency free-standing catalysts, super capacitors, electrochemical sensors, and surface-enhanced Raman scattering (SERS) substrates. A SERS application of the Au microsheets is also demonstrated.

Introduction

Nano porous gold (NPG) films have widely been an excellent candidate for applications of oxidative catalysts^{1–4}, energy storage devices,^{5–7} biosensors,^{8–10} actuator technologies,^{11,12} biomaterials for drug delivery,¹³ and surface-enhanced Raman scattering (SERS).^{14,15} There were several methods to produce NPG films.^{16–20} For example, NPG film was fabricated on titanium surface by the chemical reduction of Au precursor under a hydrothermal condition at 180°C, and then the structures were annealed at 250°C under argon protection in order to increase the porosity of structures.^{9,21} Another method is silver dealloying. In this method, Au/Ag alloy or blended Au/Ag powders were immersed into HNO₃ in order to selectively dealloy Ag from Au structures.^{2,10,22–25} However, the annealing process at 600°C is still required at the final step. Direct imprinting technique can shape the obtained NPG films for tuning desirable properties.¹⁴ The templating technique is

another conventional technique to fabricate NPG. A template such as SiO₂ nanoparticles and porous alumina is built, and then metal is deposited into a cavity of a template using various methods, *e.g.*, electrochemical deposition.^{26–28} Finally, the template is etched or dissolved to release a free structure of NPG. Nevertheless, dynamic template such as hydrogen bubbles was employed in order to avoid a template-etching procedure.²⁹

Galvanic replacement is one of the several methods to prepare isolated NPG particles, *e.g.*, porous gold nanowires, gold nanocages, and cubic Au nanoframes.^{30–32} It is a spontaneous electrochemical reaction, which can be used to fabricate Au films on surfaces of Si and Ge.^{33–37} By Galvanic replacement, metal ions are reduced to zero-charge metal by receiving electrons from other sacrificed metal templates. In addition, the structures of built metals would contain the structures of sacrificed templates. The standard reduction potentials of sacrificed metal templates play an important role in this method. Only metal ions that have higher standard reduction potentials than sacrificed metal template can be reduced and deposited on the surface of a sacrificed metal template. For example, the reduction potential of Au³⁺/Au half-cell is 0.99 V vs. standard hydrogen electrode (SHE) while Ag⁺/Ag pair contains the standard reduction potential of 0.80 V vs. SHE.³¹ Therefore, Au³⁺ can be reduced to Au⁰ by a sacrificed electron from the Ag templates, as follows:



^a Sensor Research Unit, Department of Chemistry, Faculty of Science, Chulalongkorn University, 254 Phayathai Road, Patumwan, Bangkok 10330, Thailand. Telephone/Fax: +662 218 7585

*Corresponding author: prompong.p@chula.ac.th

Electronic Supplementary Information (ESI) available: [Solution-exposed side SEM micrograph of Galvanized layer, SEM micrographs of Galvanized layer after NH₃ treatment, EDS mapping images of Galvanized layers, The mechanism of co-deposition process in the formation of Galvanized layers, Pore size distribution of the synthesized nano/microporous Au microsheets, EDS spectra of Galvanized flakes, Video of nano/microporous gold microsheets synthesis using ultrasonic radiation, SEM micrographs of Galvanized flakes produced with additional NaCl and the residual Ag plates, SERS application of the constructed nano/microporous Au microsheets.]. See DOI: 10.1039/x0xx00000x

From Eqs. 1 and 2, AgCl is a solid byproduct of this reaction, and the epitaxial deposition of Au atoms on Ag surface might be disturbed by the diffused AgCl in the growing sites.^{31,38} This disturbance is a key factor to promote the formation of porous Au structures.^{31,38} To adjust the degree of porosity in Au structures, temperature and chloride concentrations were controlled in previous works.^{30,31,39,40} Moreover, excess chloride ion reacts with AgCl and form silver chloride complex, which is more soluble than AgCl,⁴¹ as follows:



The ultrasonic sound/wave, which is mechanical vibrations with the frequency of 20 kHz at least, can produce expansion and compression cycles traveling through a matter in both solid, liquid, or gas. When the sound field is applied to liquid, pressure fluctuations are built up inside the liquid itself. Then, growth and collapse of microbubbles (acoustic cavitation) that create high local turbulence and the release of heat energy are generated.⁴² Hydrodynamic cavitation is a physical phenomenon of ultrasonic process that provides mechanical effects such as mixing and shearing in the liquid.^{43,44} Ultrasonic wave was employed in several works, for example, ultrasonic cleaning⁴⁵ or a versatile synthetic tool.⁴⁶⁻⁴⁹

The synthesis of nano/microporous Au microsheets has several limitations such as the requirement of block copolymer to use as the growing template,^{50,51} and a long time of the growing process.^{52,53} In this work, nano/microporous Au microsheets were successfully developed using ultrasonic-assisted cyclic Galvanic replacement reaction of Ag and Au³⁺. The synthesized nano/microporous Au microsheets contain a two-length-scale structure, which provides a dual function of facilitating mass transport by micropores and increasing surface area by nanopores.^{22,26,54} This developed method combines a chemical technique (*i.e.*, Galvanic replacement reaction) and a physical technique (*i.e.*, ultrasonic shearing) together and provides the advantages of increasing the porosity of Au structures, and reducing the reaction time (within 10 minutes at room temperature). This offers an opportunity to apply in the large synthesis batch for commercialization. The synthesized Au structures are good catalysts at low temperature,⁵⁵ good thermal stability and resistance to oxidation,^{56,57} and good catalysts without any support.⁵⁸ Also, our synthesized Au structures show a potential application in use as a good SERS substrate. By using crystal violet (CV) as a Raman dye and our synthesized Au structures as a substrate, Raman signal of CV can be strongly enhanced.

Experimental

Chemicals

Nitric acid (HNO₃, 65%), ammonia solution (NH₃, 25%), and hydrochloric acid (HCl, 37%) were purchased from Merck®. All chemicals were analytical grade and were used as received without an additional purification. Deionized water was used as a solvent. Silver plates (≥ 99.99% purity) and gold beads (≥

99.99% purity) with a diameter of 2–3 mm were purchased from a local precious metal retailer (Umicore Precious Metals (Thailand) Co., Ltd.). A solution of concentrated gold ion (0.5 M Au³⁺) in the form of tetrachloroauric (III) acid, HAuCl₄, was prepared by dissolving 10 g of gold beads in 40 mL aqua regia under a mild agitation and heating (80–100°C). When all gold beads were completely dissolved after heating for at least 10 hours, the solution was further heated until almost dried. Deionized water was added to the solution, and the volume was adjusted to 100 mL. The concentrated gold ion solution was employed as a source of gold ion for further investigation. Caution: aqua regia, a mixture of HCl and HNO₃ with a volume ratio of 3:1, is acutely toxic chemicals and should be handled with care. Prior to use, all glassware and magnetic bars were thoroughly cleaned with detergent, rinsed with deionized water, rinsed with aqua regia, and thoroughly rinsed with copious amounts of deionized water. Silver plates were ultrasonically cleaned before using.

Synthesis of nano/microporous Au microsheets

The solution of 25 mM HAuCl₄ was sonicated in an ultrasonic bath (CREST, TRU-SWEEP model 575D with a sonic power of 135 W) at room temperature. Then, sacrificed silver plate (5mm×5mm×0.08mm, ~0.02 g) was immersed into the solution. The color of silver plate immediately turned black. Within 10 seconds, a cloud of black particles spread out from the surface of silver plate (Electronic Supplementary Information, Video S1). The silver plate completely disappeared within 10 minutes. The black precipitates were obtained after removing ultrasonic source. The supernatant (the solution of excess gold ion) was removed, and the black particles were rinsed by water. The co-developed AgCl was removed by immersing the black precipitates into ammonia solution (NH₃, 10 mL, 10 % w/v) for 15 minutes. The residual ammonia was removed by rinsing the particles with a copious amount of water. The obtained nano/micro Au microsheets were dried under ambient condition and stored in a desiccator for further investigations.

Characterizations

Scanning electron microscopy (SEM). A Galvanized silver plate was attached to a stainless steel stub through a carbon tape. All SEM micrographs were recorded with a JEOL JSM-6510A operated at acceleration voltages of 10–30 kV under high vacuum mode using a secondary electron imaging (SEI). Elemental analysis was carried out using a built-in JEOL energy dispersive X-ray spectrometer (EDS) model JED 2300.

X-ray diffraction (XRD). The samples were measured using a Rigaku D/MAX-2200 instrument (Cu K_{α1} radiation) operated at 50 kV and 250 mA over the range of 30–90 degrees by a scanning step with a step size of 0.02 degree.

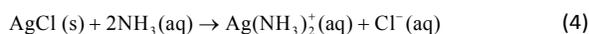
Results and discussion

Galvanic replacement reaction without ultrasonic radiation

At first, Galvanic replacement reaction of Au on sacrificed Ag substrate without ultrasonic radiation was investigated. The

reaction was initiated by dipping Ag plate into gold ion solution for 30 minutes. The generated Galvanized layer was detached from the surface of Ag plate using corneal forceps. Fig. 1(A1) shows SEM micrograph of Galvanized layer at the solution-exposed side. It reveals the connection of round-edge particles with the particle size of 1–3 μm , which are the characteristics of continuous AgCl layers.⁵⁹ Moreover, the grain boundary between AgCl particles and the microchannel with the diameter sizes of 0.5–1 μm inside particles can be observed (Electronic Supplementary Information, Fig. S1). The microchannels promote the ion transportation and increase the ionic conductivity of the whole layers.⁵⁹ This phenomenon allows the Galvanic replacement reaction to take place continuously, even the sacrificed Ag surface is fully covered with Galvanized layers.

The solid AgCl, which concurrently developed with Au nanostructures (Eq. 2), can be dissolved in ammonia solution:



After the removal of AgCl using ammonia solution, the Galvanized layer reveals the hidden coral-like Au nanostructures (Fig. 1(A2)). This layer consists of connected clusters of Au nanoribbons with the thickness of 25–50 nm (Electronic Supplementary Information, Fig. S2). The black spots on the surfaces are vacancies, which were previously occupied by AgCl microparticles. The uniformly dispersed porous structures in the Au layers indicate that Galvanized layers are formed by the co-deposition of Au and AgCl.³¹ According to Eqs. 1 and 2, the 3-time mole ratio of AgCl: Au causes AgCl to be a dominant structure and act as a hard template for the growth of coral-like Au nanostructures.

In Fig. 1(B1), side view SEM micrograph of Galvanized layer shows the thickness of Au/AgCl composite layer with 22–23 μm . The AgCl in Galvanized layer was dissolved in NH_3 solution in order to reveal the deposition pattern of Au/AgCl composite (Fig. 1(B2)). The detail structures of coral-like Au micro/nanostructures after AgCl removal is illustrated by a side view vertical panorama SEM micrograph in Fig. 1(B3). The condensed area of Au structures can be observed at < 300 nm from the lower bound of Galvanized layer (Ag-attached side) and the structures with micro pores could be noticed at above 500 nm from the lower bound. The density of Au structures decreases when the Galvanized layer grows further to be a thicker layer. It suggests that the epitaxial deposition firstly occurs on a surface of Ag plate with the high density of Au structures because of a small difference in lattice constants ($\text{Au} = 0.408 \text{ \AA}$, $\text{Ag} = 0.409 \text{ \AA}$).⁴⁴

Moreover, the gradient of the Au structure density can be observed along the thickness of Galvanized layer (Fig. 1(B3)), which is a good evidence of Cl^- concentration effect on the formation of Au/AgCl composites. After immersing sacrificed Ag plate into HAuCl_4 solution, Ag atom starts to be oxidized and Ag^+ ion is produced. Under very high concentration of Cl^- and very low pH conditions (in the solution of HAuCl_4), very soluble silver chloride ion complexes ($\text{AgCl}_n^{(n-1)-}$) can be formed immediately (as expressed in Eq. 3), while a small amount of AgCl are generated. As a result, a small number of AgCl co-

deposition occurs during an epitaxial deposition of Au on Ag surface. This results the high density of Au structure at the lower bound of Galvanized layer (Ag-attached side).

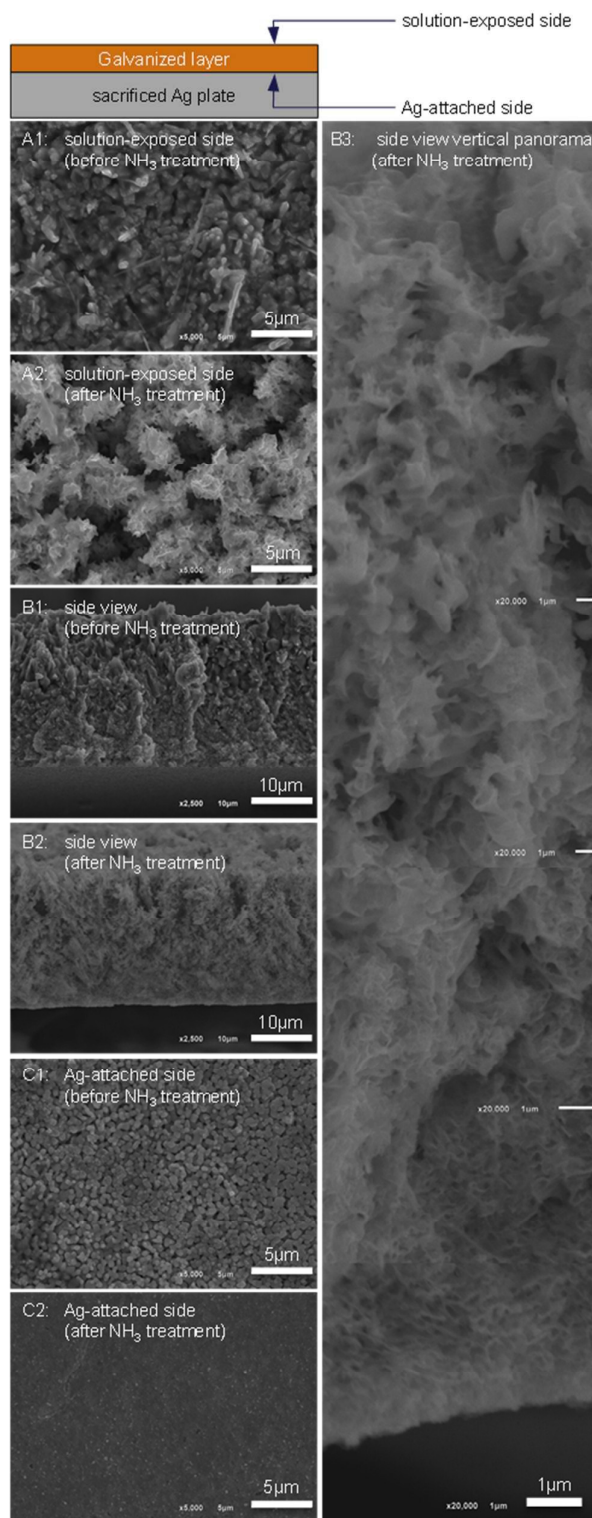


Fig.1 (A) solution-exposed side, (B) side view, and (C) Ag-attached side SEM micrographs of Galvanized layer (A1, B1, C1) before and (A2, B2, C2) after NH_3 treatment. (B3) Side view vertical panorama SEM of Galvanized layer after NH_3 treatment.

However, the low density of Au structures with microporous structures can be observed at the top part of the Galvanized layer (closed to solution-exposed side) because, at the late of reaction, more Ag atoms are oxidized to Ag^+ ions, which produce more AgCl to co-deposit with Au atoms. If there is no effect from Cl^- concentration on the formation of Au/AgCl composites, the Au structure density should be similar thorough the layer.

The SEM micrographs of Galvanized layer at Ag-attached side before and after NH_3 treatments are also shown in Fig. 1(C). They indicate that the round-edge particles covering whole Ag-attached surface of Galvanized layer are AgCl, which was removed by soaking in NH_3 solution. Due to the formation of these AgCl underlayers, the Galvanized layer can be easily detached from a surface of Ag plate by external mechanical force.

The formation of AgCl underlayers

The formation of AgCl underlayers was investigated by observing time-dependent side view SEM micrographs of Galvanized layer, as shown in Fig. 2. At the first 5 seconds of Galvanic replacement reaction, the color of Ag plate changes to black with the formation of Galvanized layer. The co-deposited Au/AgCl clusters with the size of 150–300 nm can be observed on the surface of Ag plate, and the thickness of this co-deposition layer is approximately 700–800 nm (Fig. 2(A1)). At this stage, the Galvanized layer cannot be detached from a Ag surface due to a strong epitaxial adhesion between Au and Ag. An insignificant change in the morphology of the layer after NH_3 treatment (Fig. 2(A2)) indicates that this layer is mainly Au. After 60 seconds, the layer can be easily removed from a Ag surface by an external mechanical force because of the immiscibility between AgCl and Ag (Fig. 2(B)). The thickness of the Galvanized layer obtained at the 60-second reaction time is approximately 2.6–3.0 μm (Fig. 2(B1)), which is reduced to 1.9–2.3 μm after NH_3 treatment (Fig. 2(B2)). It indicates that the layer consists of a large proportion of AgCl generated during this period.

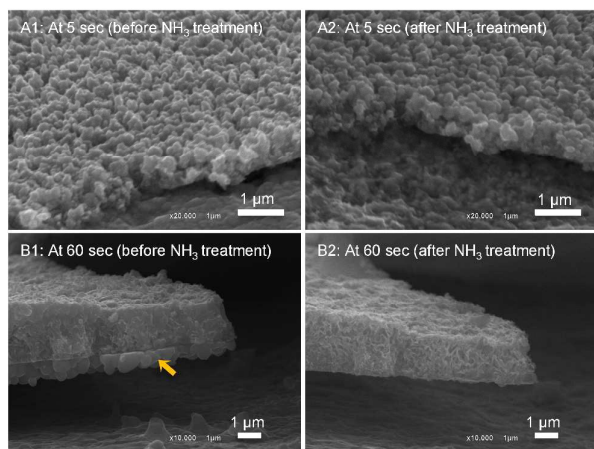


Fig. 2 Side view SEM micrographs of Galvanized layer at (A) 5- and (B) 60-second reaction time (A1, B1) before and (A2, B2) after NH_3 treatments. The arrow points at AgCl underlayer.

EDS spectra of Galvanized layers, which were collected at the 30-minute reaction time, before and after NH_3 treatments are shown in Fig. 3. In Fig. 3(A), strong peaks at 2.21, 2.62, and 2.98 are attributed to $\text{Au}_{M\alpha}$, $\text{Ag}_{K\alpha}$, and $\text{Cl}_{L\alpha}$, respectively. Using a conventional ZAF procedure, the Au, Ag, and Cl compositions of Galvanized layer before NH_3 treatment are calculated to 6.98, 49.28, and 43.74 % atoms, respectively. After NH_3 treatment, EDS result shows that the content of Au in the layer increases to 93.94 %. It is an evidence of AgCl removal. No Cl atom can be detected, and the content of Ag decreases to 6.06 %. The Ag residues possibly occur from the reduction of Ag^+ , which is generated during the Galvanic replacement reaction, then grow and widely spread in the Au structures. EDS mapping images that reveal the distribution of Au, Ag, and Cl in Galvanized layers before and after NH_3 treatments are presented in Electronic Supplementary Information, Fig. S3.

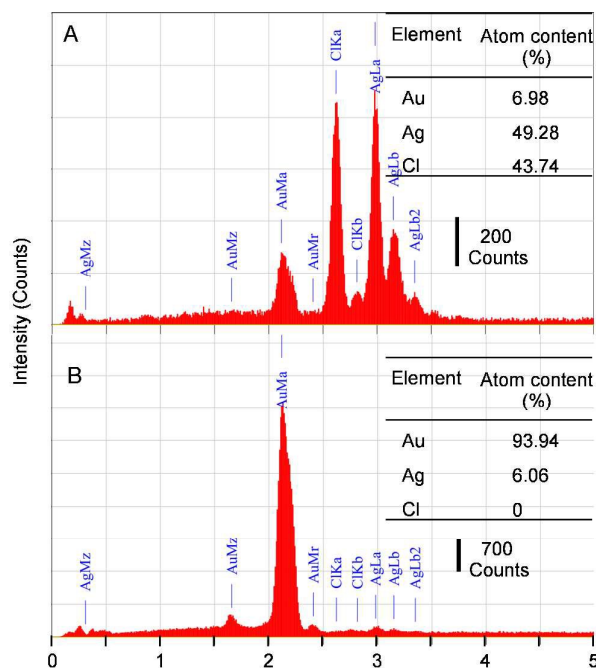


Fig. 3 EDS spectra of Galvanized layers (A) before and (B) after NH_3 treatments.

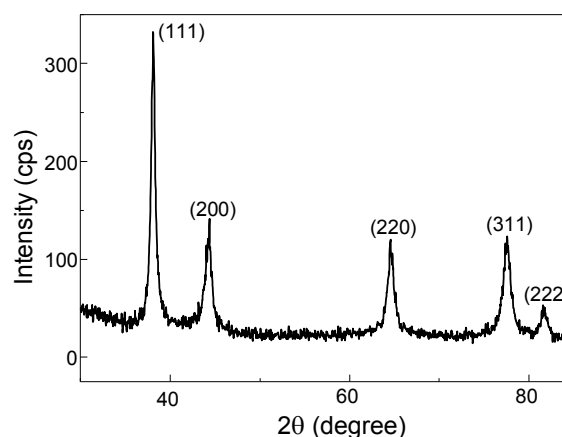


Fig. 4 XRD pattern of coral-like gold nanostructures after NH_3 treatment.

Fig. 4 shows XRD pattern of coral-liked Au micro/nanostructures after NH_3 treatment. The peaks at 2 θ of 38, 44, 64, and 77 degrees are contributed to crystal orientation planes of (111), (200), (220), and (311), respectively, which represent a face-centered cubic lattice of Au.^{28,60,61} It is worth mentioning that the intensity ratio of (200) plane to (111) plane for coral-liked Au structures is 0.42, which is lower than that of common Au powder (0.52).^{62,63} This suggests that coral-liked Au structures contain more numbers of (111) plane than a normal Au structure, which implies that the facet of Au nanoplates in coral-liked Au structures is mainly a (111) plane.

The mechanism of co-deposition process in the formation of Galvanized layers is depicted in Electronic Supplementary Information, Fig. S4. Since Galvanic replacement reaction always takes place at the interface between a solution of Au^{3+} ions and a sacrificed Ag metal, the oxidation reaction firstly arises on a Ag surface (anode) to generate Ag^+ and free electron (e^-). While electron is transferred to the aqueous phase and allows the reduction of Au^{3+} , the produced Au atoms are deposited on a sacrificed Ag surface. From Eq. 2, Ag^+ and Cl^- , which are byproducts of Galvanic replacement reaction, combine together and form AgCl precipitates with the Au:AgCl mole ratio of 1:3. Then, AgCl precipitates deposit on Ag surface,³¹ and continuously co-deposit with Au atoms to form a film (Fig. S4(B)). To build up further structures, an electron from the oxidation at Ag anode is transferred *via* the connected Au structures, which are previously produced, to the top surface of Galvanized layers (solution-exposed side). Subsequently, AuCl_4^- is reduced to Au atom by receiving this electron, and Au atom deposits and grows on the surface of previously grown Au layers. Furthermore, microchannels, which are a characteristic of AgCl structure (Electronic Supplementary Information, Fig. S1), are created at this period and play an important role to transfer ions (Au^{3+} , Ag^+ , and Cl^-) through Galvanized layers (Figs. S4(C)–S4(D)). When Galvanic replacement undergoes, Ag surface is gradually eroded, and a gap between sacrificed Ag surface and Galvanized layer is increasingly developed. Therefore, Cl^- can diffuse into this gap and react with Ag^+ from the oxidation of sacrificed Ag surface to form AgCl underlayers, which deposits at the bottom of Galvanized layer (Figs. S4(D)–S4(E)). It is in good agreement with SEM micrographs of Galvanized layers before and after NH_3 treatments in Figs. 1–2 that indicate the existence of AgCl underlayers at the bottom of Galvanized layers (Ag-attached side). From the proposed mechanism, only large Au microsheets with porous structures can be synthesized through the chemical reaction. Moreover, the Galvanic reaction is terminated after the surface of Ag plate is fully covered with AgCl underlayers, leading to the remains of residual Ag plate.

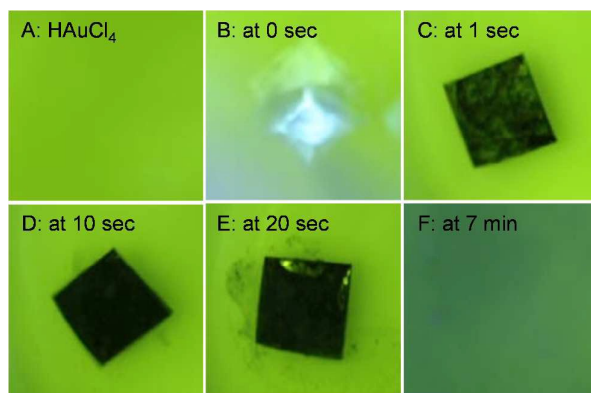


Fig.5 Time-dependent images of Ag plates dipped in HAuCl_4 solution under ultrasonic irradiation. (A) A HAuCl_4 solution before Galvanic replacement reaction (B–E) Galvanic replacement reaction at 0 sec, 1 sec, 10 sec, 20 sec, and 7 min of reaction time, respectively.

Synthesis of nano/microporous gold microsheets using ultrasonic radiation

By applying ultrasonic radiation during the Galvanic replacement process, the Galvanized layers were immediately detached from a sacrificed Ag surface when the layers were formed. Fig. 5 shows time-dependent images of Ag plates dipped in HAuCl_4 solution under ultrasonic radiation. The video of this synthesis is also shown in Electronic Supplementary Information, Video S1. After dipping sacrificed Ag plate into HAuCl_4 solution, the color of Ag surface rapidly changes to black within a second, as shown in Figs. 5(A)–5(C). At the early stage of the reaction, the epitaxial deposition of Au atoms occurs, and the black Galvanized layers are developed at the sacrificed Ag surface. There is no significant difference between the reaction with and without ultrasonic radiation at this period. However, at the late stage of reaction (after 10 seconds of reaction time, Figs. 5(D)–5(E)), the black particles from a surface of Ag plate were scrubbed into the solution. At this period, AgCl underlayers grow at the bottom of the Galvanized layers, as described above in Figs. 1, 2, and S4. The growth of these AgCl underlayers causes a decrease in the miscibility between Galvanized layers and a sacrificed Ag surface due to the cavitation of gaps and grains in the AgCl structures. When ultrasonic wave interacts with the plate, the Galvanized layers are ejected from a sacrificed Ag surface. This phenomenon is the same as that in a normal ultrasonic cleaning procedure. Finally, the Galvanized flakes ceaselessly disperse from the plate into the solution until no sacrificed Ag plate supplies electrons for further Galvanic replacement reaction (Fig. 5(F)).

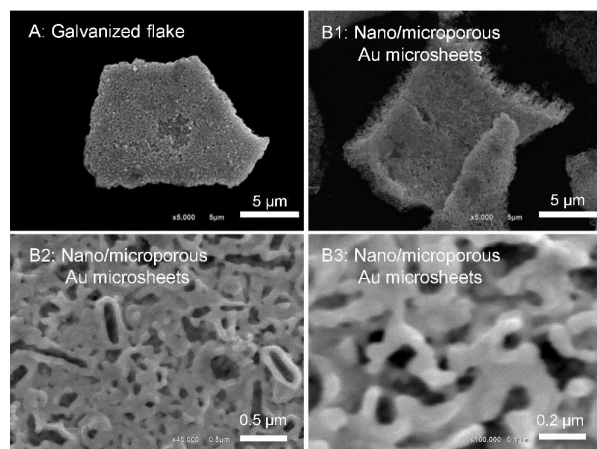


Fig. 6 SEM micrographs of (A) Galvanized flake ejected from sacrificed Ag plate and (B) porous Au micro/nanostructures after NH_3 treatment.

The Galvanized flakes that are split from sacrificed Ag plate were investigated using SEM measurement before and after NH_3 treatments, and their SEM micrographs are presented in Fig. 6. The lateral sizes of Galvanized flakes are approximately 5–10 μm , and the thickness is in the range of 0.5–1.0 μm , as illustrated in Fig. 6(A). After detaching AgCl from the flakes using NH_3 treatment, porous Au micro/nanostructures were obtained (Fig. 6(B1)). In Figs. 6(B2) and 6(B3), the micropores and nanopores with the size of 0.15–0.30 μm and 30–60 nm, respectively, in the structures of Au microsheets can be observed. By measuring 645 pores in Au microsheets, the ratio of pore number between micro (>100 nm) and nano (<100 nm) pores is 0.66. Therefore, nano pore is predominant in the synthesized Au microsheets (Electronic Supplementary Information, Fig. S5). The changes in compositions of Galvanized flakes before and after NH_3 treatments were investigated using EDS spectra, as shown in Electronic Supplementary Information, Fig. S6. The results show the same morphologies and compositions as those of Galvanized layers produced without ultrasonic radiation. In addition, the existence of AgCl underlayers at the bottom of Galvanized flakes is also evidenced.

Cyclic Galvanic replacement mechanism

Fig. 7 depicts the schematic diagram of cyclic Galvanic replacement reaction for the formation of Galvanized flakes. At first, a clean sacrificed Ag surface is supplied. The sacrificed Ag surface in the presence of AuCl_4^- allows the rapid epitaxial growth of Au film on the clean Ag surface. The Cl^- is a byproduct of this Galvanic reaction, reacts with the Ag^+ generated by the oxidation of Ag surface, and then forms AgCl precipitates on the surface of previously generated Au film. By this Au/AgCl co-deposition, the interpenetrated Au/AgCl nanocomposites are later formed. When a gap between a Galvanized layer and a Ag surface is created by an oxidative deterioration of Ag surface, Cl^- diffuses into this gap and reacts with Ag^+ dissolved from Ag surface to develop AgCl underlayers at the interface between a Galvanized layer and a Ag surface. After a AgCl underlayer develops and covers over

the interface, the Galvanic-generated interpenetrated Au/AgCl nanocomposite film with the AgCl underlayer is detached from the sacrificed Ag surface by an assistance of ultrasonic radiation. The ultrasonic-assisted auto-detachment enables a self-initiated formation of a clean Ag surface on a Ag plate. This self-regeneration enables cyclic formation of Au/AgCl nanocomposite film with the AgCl underlayer until the Galvanic reaction completely consumes the Ag plate.

However, the cyclic Galvanic replacement would be inhibited by excessive Cl^- . With the addition of NaCl, the formation of Galvanized flakes can be observed at the early stage. Then, the surface of Ag plate is covered with AgCl, which is generated from dissolved Ag^+ and added Cl^- . The generated AgCl on a surface of Ag plate protects the Ag surface from the oxidation. Therefore, $\text{Au}^{3+}/\text{Ag}^+$ Galvanic reaction does not undergo, and the cyclic Galvanic replacement is terminated, which causes the remains of Ag plates covered by AgCl. The Galvanized flakes produced with additional NaCl, and the residual Ag plates are shown in Electronic Supplementary Information, Tables S1–S2.

SERS application

Additionally, SERS application of the constructed nano/microporous Au microsheets is demonstrated in Electronic Supplementary Information, Fig. S7. Crystal violet (CV), which is a common Raman dye, was employed as a molecular probe to investigate the enhancement of Raman signal. The results show that SERS signal of CV is enormously stronger than normal Raman signal of CV. The rise of Raman signal enhancement is due to porous structures in Au microsheets, which provide a large number of “hot-spot” with high electric field. This high electric field couples with the incident and scattering light on the surface of Au microsheets, and then produce strong Raman scattering signal of adsorbed molecules. Moreover, the pores in Au microsheets also increase the surface area for the adsorption of molecules, which slightly improves Raman intensity. The enhancement factor (EF) of the constructed nano/microporous Au microsheets can be calculated to 6.1×10^7 (the calculation detail is described in Electronic Supplementary Information). It suggests that synthesized nano/microporous Au microsheets are a good candidate for using as a sensitive SERS substrate.

By observing SEM images in Fig. 6, a porous structure is quite uniform throughout Au microsheets. The uniformity of Au microsheets is good enough to use them as a SERS substrate because the smallest size of laser spot in a conventional Raman spectrometer is approximately 1 μm , which covers whole Au microsheets.

The morphology and porosity of Au microsheets mainly depend on the nature of the co-precipitation of Au/AgCl and the Galvanic replacement of Ag/Au^{3+} . Especially, the co-precipitation process plays an important role to build porous structure in Au microsheets. Using the proposed technique, we found that the concentration of any reagents does not affect the morphology and porosity. However, it is possible to control the co-precipitation and Galvanic replacement processes by

adjusting the temperature of synthesis. Moreover, applying different power of ultrasonic radiation may give different auto-

detachment of Galvanized flake, which may also cause differences in the morphology and porosity.

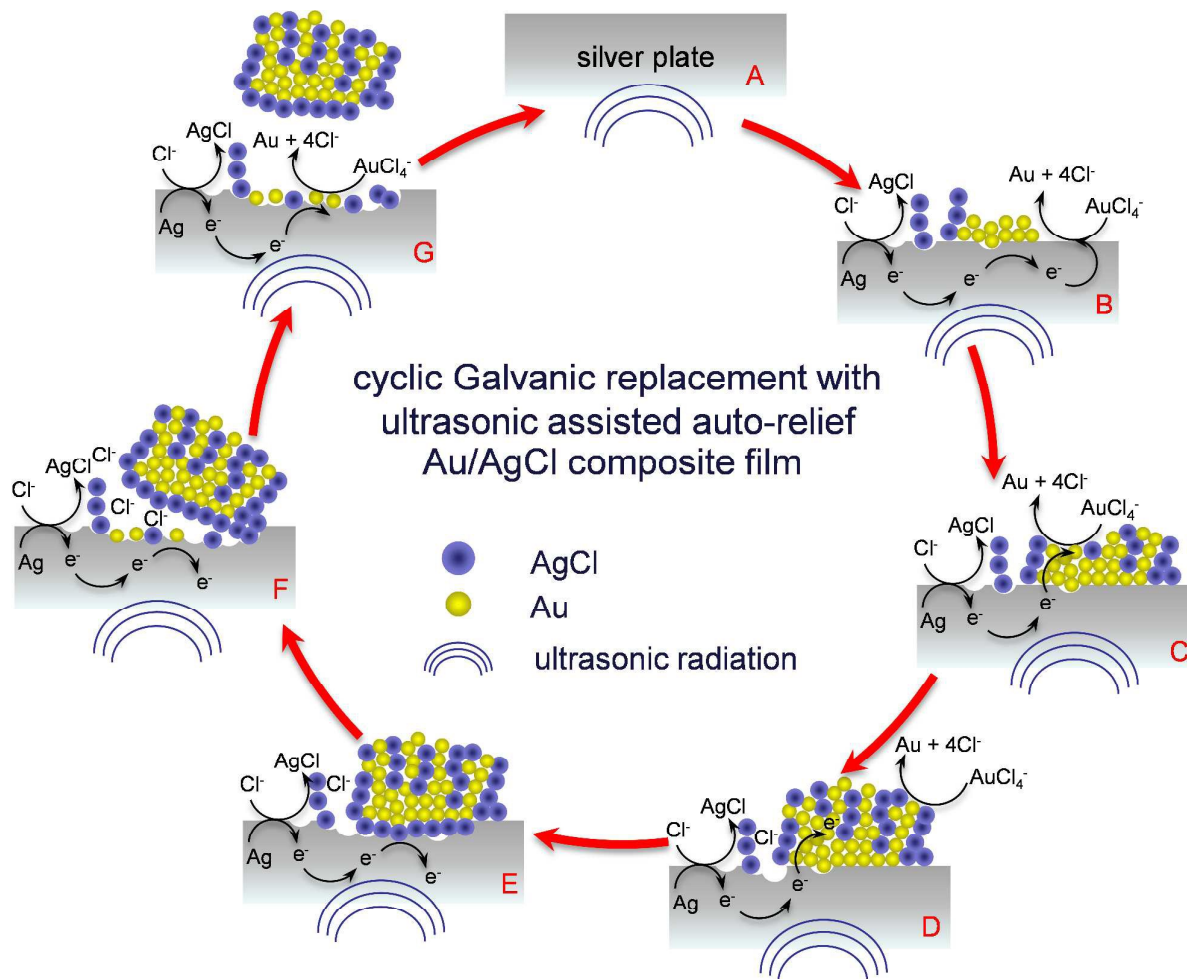


Fig.7 Proposed cyclic Galvanic replacement for the formation of nano/microporous Au microsheets. (A) Supply/regeneration of a clean Ag surface. (B) Rapid epitaxial growth of Au film on the clean Ag surface. (C) Precipitation and formation of AgCl precipitates on Au film. (D) Formation of interpenetrated Au/AgCl nanocomposites. (E) Development of AgCl underlayer. (F) Ultrasonic-assisted detachment of the interpenetrated Au/AgCl nanocomposite film with a AgCl underlayer.

Conclusions

Nano/microporous Au microsheets are successfully fabricated using ultrasonic-assisted cyclic Galvanic replacement technique. Any capping agent, template, or stabilizer is not necessary for this synthesis method. The pores in free standing micrometer-sized Au film are created by a AgCl byproduct, which co-deposited with Au. AgCl underlayer is a key factor for the detachment of Galvanized layer from Ag surface under ultrasonic irradiation. The advantages of this fabrication method are a simple procedure with low synthetic cost, no requirement for expensive and complex instrument, the high increment of porosity in Au structures, short reaction time (within 10 minutes at room temperature), and the possibility for large-scale production. Moreover, the fabricated structures could provide potential applications for using as SERS substrates and catalysts.

Acknowledgements

This research has been supported by National Research University Project, Office of Higher Education Commission (WCU-018-FW-57).

References

- 1 R. Zeis, T. Lei, K. Sieradzki, J. Snyder, J. Erlebacher, *J. Catal.*, 2008, **253**, 132-138.
- 2 A. Wittstock, V. Zielasek, J. Biener, C.M. Friend, M. Bäumer, *Science*, 2010, **327**, 319-322.
- 3 L.C. Nagle, J.F. Rohan, *Int. J. Hydrogen Energy*, 2011, **36**, 10319-10326.
- 4 C. Xu, X. Xu, J. Su, Y. Ding, *J. Catal.*, 2007, **252**, 243-248.
- 5 X.Y. Lang, H.T. Yuan, Y. Iwasa, M.W. Chen, *Scripta Mater.*, 2011, **64**, 923-926.
- 6 F. Meng, Y. Ding, *Adv. Mater.*, 2011, **23**, 4098-4102.

- 7 X. Lang, L. Zhang, T. Fujita, Y. Ding, M. Chen, *J. Power Sources*, 2012, **197**, 325-329.
- 8 K. Bonroy, J.M. Friedt, F. Frederix, W. Laureyn, S. Langerock, A. Campitelli, M. Sára, G. Borghs, B. Goddeeris, P. Declerck, *Anal. Chem.*, 2004, **76**, 4299-4306.
- 9 A.K.M. Kafi, A. Ahmadalinezhad, J. Wang, D.F. Thomas, A. Chen, *Biosens. Bioelectron.*, 2010, **25**, 2458-2463.
- 10 O.V. Shulga, K. Jefferson, A.R. Khan, V.T. D'Souza, J. Liu, A.V. Demchenko, K.J. Stine, *Chem. Mater.*, 2007, **19**, 3902-3911.
- 11 J. Biener, A. Wittstock, L.A. Zepeda-Ruiz, M.M. Biener, V. Zielasek, D. Kramer, R.N. Viswanath, J. Weissmüller, M. Bäumer, A.V. Hamza, *Nat. Mater.*, 2009, **8**, 47-51.
- 12 D. Kramer, R.N. Viswanath, J. Weissmüller, *Nano Lett.*, 2004, **4**, 793-796.
- 13 E. Seker, Y. Berdichevsky, K.J. Staley, M.L. Yarmush, *Adv. Healthcare Mater.*, 2012, **1**, 172-176.
- 14 J.D. Ryckman, M. Liscidini, J.E. Sipe, S.M. Weiss, *Nano Lett.*, 2010, **11**, 1857-1862.
- 15 J. Biener, G.W. Nyce, A.M. Hodge, M.M. Biener, A.V. Hamza, S.A. Maier, *Adv. Mater.*, 2008, **20**, 1211-1217.
- 16 G. Duan, W. Cai, Y. Luo, F. Lv, J. Yang, Y. Li, *Langmuir*, 2009, **25**, 2558-2562.
- 17 A. Fahmi, T. Pietsch, N. Gindy, *Rapid Commun.*, 2007, **28**, 2300-2305.
- 18 H. Kim, Y. Kim, *Curr. Appl. Phys.*, 2009, **9**, S88-S90.
- 19 W. Huang, M. Wang, J. Zheng, Z. Li, *J. Phys. Chem. C*, 2009, **113**, 1800-1805.
- 20 H. Zhang, J.J. Xu, H.Y. Chen, *J. Phys. Chem. C*, 2008, **112**, 13886-13892.
- 21 H. Qiu, F. Zou, *Biosens. Bioelectron.*, 2012, **35**, 349-354.
- 22 M.E. Cox, D.C. Dunand, *Mater. Sci. Eng. A*, 2011, **528**, 2401-2406.
- 23 J. Erlebacher, M.J. Aziz, A. Karma, N. Dimitrov, K. Sieradzki, *Nature*, 2001, **410**, 450-453.
- 24 C.J. Dotzler, B. Ingham, B.N. Illy, K. Wallwork, M.P. Ryan, M.F. Toney, *Adv. Funct. Mater.*, 2011, **21**, 3938-3946.
- 25 R. Laocharoensuk, S. Sattayasamitsathit, J. Burdick, P. Kanatharana, P. Thavarungkul, J. Wang, *ACS Nano*, 2007, **1**, 403-408.
- 26 W. Gao, X.H. Xia, J.J. Xu, H.Y. Chen, *J. Phys. Chem. C*, 2007, **111**, 12213-12219.
- 27 H. Gao, N.N. Gosvami, J. Deng, L.S. Tan, M.S. Sander, *Langmuir*, 2006, **22**, 8078-8082.
- 28 C.H. Wang, C. Yang, Y.Y. Song, W. Gao, X.H. Xia, *Adv. Funct. Mater.*, 2005, **15**, 1267-1275.
- 29 Y. Li, Y.Y. Song, C. Yang, X.H. Xia, *Electrochem. Commun.*, 2007, **9**, 981-988.
- 30 L. Au, Y. Chen, F. Zhou, P.H.C. Camargo, B. Lim, Z.Y. Li, D.S. Ginger, Y. Xia, *Nano Res.*, 2008, **1**, 441-449.
- 31 Y. Sun, Y. Xia, *J. Am. Chem. Soc.*, 2004, **126**, 3892-3901.
- 32 X. Lu, J. Chen, S.E. Skrabalak, Y. Xia, *Proc. Inst. Mech. Eng. N: J. Nanoeng. Nanosyst.*, 2007, **221**, 1-16.
- 33 S.Y. Sayed, F. Wang, M. Malac, A. Meldrum, R.F. Egerton, J.M. Buriak, *ACS Nano*, 2009, **3**, 2809-2817.
- 34 Y. Wang, M. Becker, L. Wang, J. Liu, R. Scholz, J. Peng, U. Gösele, S. Christiansen, D.H. Kim, M. Steinhart, *Nano Lett.*, 2009, **9**, 2384-2389.
- 35 S.Y. Sayed, J.M. Buriak, *ACS Appl. Mater. Interfaces*, 2010, **2**, 3515-3524.
- 36 A. Gutiérrez, C. Carraro, R. Maboudian, *ACS Appl Mater Interfaces*, 2011, **3**, 1581-1584.
- 37 X. Zhang, Y. Qiao, L. Xu, J.M. Buriak, *ACS Nano*, 2011, **5**, 5015-5024.
- 38 X. Lu, H.Y. Tuan, J. Chen, Z.Y. Li, B.A. Korgel, Y. Xia, *J. Am. Chem. Soc.*, 2007, **129**, 1733-1742.
- 39 S. Kwon, H. Dong, S.Y. Lee, *J. Nanomater.*, 2010, **2010**, 1-7.
- 40 M.R. Langille, M.L. Personick, J. Zhang, C.A. Mirkin, *J. Am. Chem. Soc.*, 2011, **133**, 10414-10417.
- 41 Y. Lu, Q. Wang, J. Sun, *Langmuir*, 2005, **21**, 5179-5184.
- 42 T. Leong, M. Ashokkumar, S. Kentish, *Acoustics Australia*, 2011, **39**, 54-63.
- 43 J.E. IV, W.R. Moser, B. Marshik-Guerts, *Chem. Mater.*, 1996, **8**, 2061-2067.
- 44 M. Virost, T. Chave, S.I. Nikitenko, D.G. Shchukin, T. Zemb, H. Möhwald, *J. Phys. Chem. C*, 2010, **114**, 13083-13091.
- 45 S. Muthukumar, S. Kentish, S. Lalchandani, M. Ashokkumar, R. Mawson, G.W. Stevens, F. Grieser, *Ultrason. Sonochem.*, 2005, **12**, 29-35.
- 46 Z.-Q. Li, L.-G. Qiu, T. Xu, Y. Wu, W. Wang, Z.-Y. Wu, X. Jiang, *Mater. Lett.*, 2009, **63**, 78-80.
- 47 H. Li, X. He, Y. Liu, H. Huang, S. Lian, S.-T. Lee, Z. Kang, *Carbon*, 2011, **49**, 605-609.
- 48 J.H. Bang, K.S. Suslick, *Adv. Mater.* 2010, **22**, 1039-1059.
- 49 D.G. Shchukin, D. Radziuk, H. Möhwald, *Annu. Rev. Mater. Res.*, 2010, **40**, 345-362.
- 50 R.D. Río, F. Armijo, R. Schreiber, C. Gutierrez, A. Amaro, S.R. Biaggio, *J. Solid State Electrochem.*, 2011, **15**, 697-702.
- 51 H.-M. Bok, K.L. Shuford, S. Kim, S.K. Kim, S. Park, *Nano Lett.*, 2008, **8**, 2265-2270.
- 52 W.-J. Shin, F. Basarir, T.-H. Yoon, J.-S. Lee, *Langmuir*, 2009, **25**, 3344-3348.
- 53 H.-D. Koh, N.-G. Kang, J.-S. Lee, *Langmuir*, 2007, **23**, 12817-12820.
- 54 E. Detsi, S. Punzhin, J. Rao, P.R. Onck, J.T.M. De Hosson, *ACS Nano*, 2012, **6**, 3734-3744.
- 55 C. Xu, J. Su, X. Xu, P. Liu, H. Zhao, F. Tian, Y. Ding, *J. Am. Chem. Soc.*, 2007, **129**, 42-43.
- 56 V. Zielasek, B. Jürgens, C. Schulz, J. Biener, M.M. Biener, A.V. Hamza, M. Bäumer, *Angew. Chem. Int. Ed.*, 2006, **45**, 8241-8244.
- 57 M.M. Biener, J. Biener, A. Wichmann, A. Wittstock, T.F. Baumann, M. Bäumer, A.V. Hamza, *Nano Lett.*, 2011, **11**, 3085-3090.
- 58 A. Wittstock, B. Neumann, A. Schaefer, K. Dumbuya, C. Kübel, M.M. Biener, V. Zielasek, H.-P. Steinruck, J.M. Gottfried, J. Biener, A. Hamza, M. Bäumer, *J. Phys. Chem. C*, 2009, **113**, 5593-5600.
- 59 H. Ha, J. Payer, *Electrochim. Acta*, 2011, **56**, 2781-2791.
- 60 L. Lu, I. Randjelovic, R. Capek, N. Gaponik, J. Yang, H. Zhang, A. Eychmüller, *Chem. Mater.*, 2005, **17**, 5731-5736.
- 61 Y. Xia, Z. Shi, Y. Lu, *Polymer*, 2010, **51**, 1328-1335.
- 62 B.K. Jena, C.R. Raj, *J. Phys. Chem. C*, 2007, **111**, 15146-15153.
- 63 D. Wang, J. Huang, Y. Liu, X. Han, T. You, *J. Nanopart. Res.*, 2011, **13**, 157-163.